 CMES, vol.36, no.3, pp.243-260, 2008

A Parameter Free Cost Function for Multi-Point Low Speed Airfoil Design

G. Veble[1,2,3]

Abstract: A simple cost function is proposed that depends on the inviscid pressure distribution around an airfoil and that, when minimized, results in airfoils that promote laminar flow. Additional constraints specify the design point of the airfoil. The method allows for straightforward inclusion of multiple design points. The resulting airfoils are quantitatively similar to those already successfully used in practice.

Keyword: aerodynamics, optimization, boundary element method

1 Introduction

In an attached incompressible flow over an airfoil at high Reynolds numbers, the thin boundary layer behaviour is driven by the pressure distribution as given by a largely inviscid flow around the airfoil away from the boundary layer [Anderson Jr. (2007)] . The thickness of the boundary layer decreases with increasing the Reynolds number, making the inviscid solution valid ever closer to the airfoil boundary. One of the most important features of the boundary layer flow is the fact that severe adverse pressure gradients, that occur due to the slowing down of the nearby inviscid component of the flow, promote separation of the flow from the surface. While a detached flow might reattach further downstream, it will nevertheless disturb a possibly laminar airflow and cause a transition to turbulence. For laminar airfoil design with minimum drag it is therefore essential that the point of the pressure gradient reversal is moved as far downstream as possible in order to promote laminar airflow along most of the surface, while still allowing for a gradual recovery of the pressure to the freestream value close to the trailing edge.

For a given required lift value, such requirements demand pressure distributions

[1] Faculty of Applied Sciences, University of Nova Gorica, Vipavska 13, PO Box 301, Rožna dolina, SI-5000 Nova Gorica, Slovenia
[2] Pipistrel d.o.o. Ajdovscina, Goriska cesta 50a, SI-5270 Ajdovscina, Slovenia
[3] CAMTP, University of Maribor, Krekova 2, SI-2000 Maribor, Slovenia

that quickly reach an almost constant value of negative pressure in the downstream direction along both the upper and lower parts of the airfoil, and then from a certain point drop in a gradual way towards the trailing edge [Anderson Jr. (2007)]. Such a design creates a relatively low peak (negative) pressure value in order to allow for the adverse pressure gradient region close to the trailing edge to be as short as possible. Low peak negative pressure is, on the other hand, also a welcome feature for the design of transonic airfoils, as this delays the formation of shocks. The requirements for both laminar and transonic airfoils are therefore quite similar in terms of the desired pressure distributions.

It is possible to design airfoils with specified pressure distributions via inverse methods [Lighthill (1945); Strand (1973); Selig and Maughmer (1992)]. These distributions can not be arbitrary but must satisfy certain constraints due to the fact that the pressure distributions must correspond to an actual flow. There may also be additional constraints imposed by the designer, such as the profile thickness. Designing pressure distributions that satisfy all these constraints is not entirely straightforward.

The goal of the work presented here is to avoid having to explicitly specify a desired pressure distribution when designing an airfoil. Instead, a simple cost function is proposed that, when minimized, leads to inviscid and incompressible pressure distributions with the desired properties as outlined above. The proposed cost function, which leads to airfoils quantitatively similar to the ones already used in practice, is parameter free. The parameters determining the airfoil characteristics enter the computation via straightforward design constraints such as specified lift coefficient. Using a cost function approach allows these constraints to be handled naturally by using standard approaches for constrained minimization.

Optimization problems [Nocedal and Wright (2007), Papalambros and Wilde (2000)] are an active field of research in themselves, and occur in various contexts such as fluid dynamics [Medic, Mohammadi, Petruzzelli, Stanciu, and Hecht (1999), Amirante, Catalano, Dadone, and Daloiso (2007)], structural optimizations [Fedelinski and Gorski (2006), Lamberti and Pappalettere (2007)], electrical engineering [Jimenez-Octavio, Lopez-Garcia, Pilo, and Carnicero (2008)] and new approaches towards uncertain optimization are studied [Jiang and Han (2007)].

Another advantage of using a cost function approach is evident when dealing with a multi point design. Creating an airfoil that performs best at more than a single angle of attack by using the usual inverse design methods requires the designer to specify various pressure distributions for different angles of attack that are all closely constrained by one another, making this a nontrivial task. On the other hand, a cost function based approach merely requires that all pressure distributions for various angles of attack minimize a (weighted) sum of possibly identical cost functions for

all angles of attack, without specifying in advance what the distributions should be like.

The value of the proposed method lies especially in situations where there is a need to design a large number of similar airfoils with continuously varying design points, such as e.g. the cross sections of a propeller, as the procedure is fully autonomous and can therefore be automated. In the cases where more specific design requirements are necessary, the procedure is still valuable in that it can come up with a reasonable initial design that can then be further optimized to meet those requirements.

2 Formulation

The paper deals with pressure distributions for incompressible, ideal flows around an airfoil. Designing an airfoil with respect to inviscid pressure distributions rather than e.g. minimum drag may be a preferred method since the turbulent flow predictions are still somewhat inaccurate due to the incomplete state of the available turbulence modelling, especially as far as the laminar to turbulent transition is concerned. High Reynolds number flows around streamlined bodies feature a narrow wake and boundary layer in comparison to the body size. Outside of these areas the flow is well described by the inviscid solution, and it is this inviscid solution that governs the behaviour of the boundary layer. Designing the inviscid pressure distributions in a correct manner will therefore produce the desired boundary layers that e.g. minimize drag and prevent separation.

A cost function is sought that, when minimized, will lead to airfoils with favourable pressure distributions that feature the minimum of pressure variation, along with moderate adverse pressure gradients in the areas of the flow slowdown. Let $p = \frac{v^2}{2v_0^2}$ be the dimensionless negative pressure variable, where v is the tangential velocity of the ideal fluid at the airfoil surface and v_0 is the freestream velocity. The chosen cost function is calculated as a functional of the obtained pressure distribution as

$$f(\mathbf{z},\mathbf{w}) = \int_0^L dl \left| \frac{d}{dl} p(\mathbf{z},\mathbf{w};l) \right|. \tag{1}$$

The variable $l = s/c$ is the ratio between the counter-clockwise arc length along the airfoil surface starting and the chord of the airfoil c. The variable l goes from 0 at the top of the trailing edge to L at the bottom of the trailing edge. The vector $\mathbf{z}$ represents the set of optimization variables with respect to which the cost function is minimized. The vector $\mathbf{w}$ denotes any possible additional variables which can be used to specify the design point for the airfoil, but which are not varied during minimization and will therefore often be omitted in the following text. It is important

to stress that there are no free parameters in this cost function. Since a parameter free cost function can lead to only a single optimal solution, different solutions are obtained by specifying additional constraints that depend on the desired airfoil properties.

The reasoning for choosing such a pressure functional is as follows. It is clear that the integral above can be evaluated on each interval where the sign of the pressure gradient is constant. If the points l_j denote the set of all r zeros of the pressure gradient $\frac{dp}{dl}(l_j) = 0$ together with with $l_0 = 0$ and $l_{r+1} = L$, then the integral can be evaluated as

$$f(\mathbf{z}, \mathbf{w}) = \sum_{j=0}^{r} \left| p(\mathbf{z}, \mathbf{w}; l_{j+1}) - p(\mathbf{z}, \mathbf{w}; l_j) \right|. \tag{2}$$

In an exact inviscid calculation the pressure at the cusped trailing edge is equal to 0 for any nonzero angle between the upper and lower surfaces of the airfoil, as the velocity close to that point drops to 0. In a numerical implementation of the cost function, due to discretization, the jump from 0 pressure to the one calculated at the actual trailing edge panel must be added.

In order to minimize this cost function, the corresponding pressure distribution should have as few pressure gradient reversals as possible. The differences in pressure on each subinterval should also be minimal. This should favour pressure distributions that are as uniform as possible. It is therefore expected that the above cost function will lead to the desired airfoil designs.

The procedure is, however, incomplete without specifying the constraints. Only by constraining the solution space will the minimization converge to a regular and reasonable solution. Such constraints are, for example, a specified section lift coefficient and the maximum thickness of the airfoil, but also the constraints that limit the adverse pressure gradients.

The design problem expressed as a general cost function minimization makes an extension to multi-point design quite natural. It is proposed here that multi point design should be performed by specifying a base design point at given lift and thickness constraints, and then allowing for variations in some problem parameters (usually the angle of attack) with respect to the base point. The cost function should then be given as a weighted sum

$$\tilde{f}(\mathbf{z}, \mathbf{w}) = f(\mathbf{z}, \mathbf{w}) + \sum_{k=1}^{d} \rho_k f(\mathbf{z} + \Delta\mathbf{z}_k, \mathbf{w} + \Delta\mathbf{w}_k) \tag{3}$$

where d is the number of extra design points. The offsets of the minimization variables $\mathbf{z}$ at the design point k from the base design point are given by $\Delta\mathbf{z}_k$, which

are some given constants, and similarly for the design point variable offsets $\Delta\mathbf{w}_k$. The weights ρ_k represent the relative contributions of each design point to the total cost function. Note that the change in the design point can be specified by offsetting not only the constants $\mathbf{w}$ but also the minimization variables $\mathbf{z}$. For example, this allows for the airfoil to be optimized with respect to various offset angles of attack, with the angle of attack at the base design point being a minimization variable itself.

While this is not a multiple design point optimization in the sense of being able to tailor various airfoil segments and pressure details to satisfy very specific requirements at different design points, it is nevertheless demonstrated that the multiple design point procedure as described above yields airfoils with good performance at the basic design point with a biased operating window towards the design points with less significant weights.

3 Implementation

In order to perform the optimization the airfoil shape needs to be specified as a smooth function of a finite number of variables. An arbitrary smooth airfoil shape can be represented as

$$y(x) = \pm\tau_n(x)\frac{3(1-x)\sqrt{3x}}{2} + \zeta_n(x),\ x \in [0,1], \tag{4}$$

where the signs correspond to the top and the bottom segments of the airfoil and where both the thickness function $\tau_n(x)$ and the camber function $\zeta_n(x)$ are represented by the n-th order Bézier polynomials [Bartels, Beatty, and Barsky (1998)]

$$\tau_n(x) = \sum_{i=0}^{n} T_{i,n} b_{i,n}(x), \tag{5}$$

$$\zeta_n(x) = \sum_{i=1}^{n-1} C_{i,n} b_{i,n}(x), \tag{6}$$

with Bernstein basis polynomials

$$b_{i,n}(x) = \left(\begin{array}{c} n \\ i \end{array} \right) x^i (1-x)^{n-i}. \tag{7}$$

The 0-th and n-th control point are set to 0 for the camber shape so that the chord of the airfoil always coincides with the x axis. The cost function is minimized with respect to the variables $T_{i,n}$ and $C_{i,n}$.

The Bézier polynomials have a useful feature that their order n can be increased by 1 while preserving the polynomial via the mapping

$$T_{i,n+1} = \frac{iT_{i-1,n} + (n+1-i)T_{i,n}}{n+1}. \tag{8}$$

This allows one to perform a basic optimization of an airfoil with respect to fewer variables and then increase the number of variables upon convergence in order to refine the optimization.

The minimization variables are chosen to be

$$\mathbf{z} = \{\alpha, T_0, T_1, \ldots T_n, C_1, C_2, \ldots C_{n-1}\}, \tag{9}$$

where α is the angle of attack, which, in the given formulation, is the angle between the incoming velocity vector and the x axis. In the problem as formulated here, the design parameter vector $\mathbf{w}$ is chosen to be empty as it is simply the angle of attack variation which is used to specify the various design points.

Two of the applied constraints are the section lift coefficient c_l and the maximum thickness of the airfoil in the y direction, $t_{\max}$. Any possible constraints can be specified as functions of the same variables as the cost function $f(\mathbf{z})$ and will be denoted by $g_j(\mathbf{z})$. In the present case this means $g_1 = c_l$ and $g_2 = t_{\max}$. The value of c_l is obtained directly from the panel method via the sum of all panel vorticities, whereas the maximum thickness calculation is performed by a Newton method search for the zero derivative of the airfoil thickness as obtained from the Eq. 4.

Another constraint will generally be required in order to promote favourable pressure recovery in the regions of adverse pressure gradient near the trailing edge. While there exist models that promote optimal pressure recovery without separation such as the Stratford pressure recovery [Liebeck and Ormsbee (1970)] or its improvements [Eppler (1991)], a model is sought here that has the general characteristics of the ideal recovery but which is local in terms of the pressure distribution is and independent of the coordinates, such that it can be generally applicable to a large class of airfoils. A model is used that can be expressed as a constraint relating pressure and its derivative of the form

$$r(\mathbf{z}) = \min_l \left\{ \theta\left(p(l)\right) \frac{d}{d\tilde{l}} p(l) + \mu \; p(l)^{\nu} \right\} = 0. \tag{10}$$

The derivation with respect to the length parameter, $d/d\tilde{l}$, is to be taken in the direction of the local fluid flow. The constant μ gives the inverse of the typical length over which the pressure recovery takes place, while ν determines how much faster the recovery takes place at larger negative pressures. The weight function θ should be equal to 1 for large negative pressures, but it should be 0 when the negative pressure approaches 0 due to the fact that, in an inviscid calculation, the pressure gradients close to the trailing edge of the airfoil will be approaching infinity for any nonzero angle of the cusp between the upper and lower surfaces, and thus the pressure gradient can not be constrained close to the values of pressure approaching 0.

The function was chosen as

$$\theta(p) = \begin{cases} p - p_0 > \delta p & ; \quad 1 \\ -\delta p < p - p_0 < \delta p & ; \quad \frac{1}{2}\left[1 + \sin\left(\frac{\pi(p-p_0)}{2\,\delta p}\right)\right] \\ p - p_0 < -\delta p & ; \quad 0 \end{cases} \tag{11}$$

where p_0 denotes the negative pressure where the constraint becomes significant and δp gives half the transition interval.

A constant vorticity panel method with a vorticity Kutta condition at the trailing edge is used to determine the velocity and hence pressure distributions around the airfoil (see Appendix A: for solution details).

A simple constrained gradient search method is employed to search for the minimum of the cost function $\tilde{f}$,. Faster converging schemes rely on the analytical behaviour of the cost function close to the minimum. They were therefore purposely avoided due to the non analytical nature of both the cost function as well as of the certain constraints.

As, due to the large number of minimization variables, the gradient computations are expensive, an approximate line search along the constrained gradient direction is performed before recalculating the gradient. For more implementation details see Appendix B:.

4 Results

The procedure as outlined in the previous section was used to obtain example airfoils for both single and multiple design points. In all the calculations shown, the order of the Bézier polynomial was $n = 9$. The number of panels in the panel method was $N = 100$, with the x coordinates that are joining the neighbouring panels being distributed according to the formula

$$x_i = w_i - \sin(2\pi w_i)/(2\pi),\ w_i = i/(N/2), \tag{12}$$

which bunches the panels close to the leading and trailing edges, where pressure variations are fastest. The obtained airfoils were then analyzed with the program XFOIL v6.96[1] [Drela and Giles (1987)], using the default parameters of the program. There were 200 panels used in the analysis, redistributed from the original coordinates within the program itself.

As an example of the design procedure, an airfoil with a primary design lift coefficient $c_l = 1$ and a thickness to chord ratio of 12% was chosen. The pressure

[1] Mark Drela's XFOIL program is distributed under the GPL licence at `http://web.mit.edu/drela/Public/web/xfoil/`

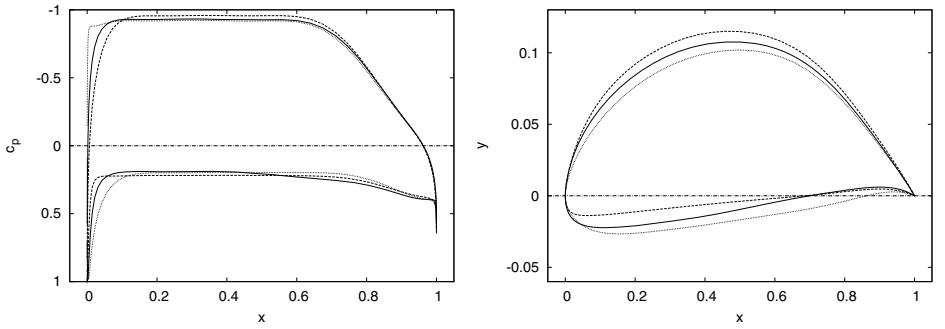

Figure 1: A series of airfoils of 12% thickness and a design lift coefficient $c_l = 1.0$. In the top picture, the pressure distribution for the case of a single design point is shown as a dotted curve, the double design point distribution is shown dashed and the triple design point is shown as a full curve ($c_p = 1 - v^2/v_0^2$). In the bottom picture, the corresponding airfoil shapes are shown. See text for details.

recovery parameters were picked as $\mu = 3$, $\nu = 1$, $p_0 = 1/2$ and $\delta p = 1/20$. The airfoil was first designed at the single design point. A double design point calculation with the offset angle of attack $\Delta\alpha_1 = 1/(4\pi)$ and the weight $\rho_1 = 1/5$ (see Eq. 3) was then performed. Finally, a triple design point calculation with an additional negative angle of attack offset $\Delta\alpha_2 = -1/(4\pi)$ and the weight $\rho_2 = 1/5$ was done. The results of these three calculations are given in Fig. 1.

The dotted curve represents the pure single point design. The minimization procedure yields a pressure distribution that, on the top surface, very quickly reaches a plateau near the leading edge. Pressure then remains constant along the length of the airfoil until the region of adverse pressure gradient is reached, where the behaviour is dominated by the adverse pressure gradient constraint as given by Eq. 10. On the bottom surface, the minimization favours a plateau in pressure as well, with two significant differences. There exists a certain amount of pressure loading both near the leading and the trailing edges of the airfoil. As the pressure distribution in this area is not affected by the pressure gradient constraint, the front and rear loading is a feature of the cost funtion (Eq. 1) itself. Since the cost function minimizes the variations in pressure, this additional loading, that alters the bottom pressure distribution only midly, occurs in order to reduce the maximum velocity on the upper surface. Such a pressure distribution favours a laminar flow, while the slow pressure recovery towards the trailing edge prevents significant airflow separation.

The dashed curve gives the pressure distribution for the double design point, where

an additional bias exists towards larger angles of attack. The weight given to the secondary design point is small enough that it does not destroy the plateaus in pressure on either side of the airfoil. The main difference to the single point design case is the reduction of the pressure loading on the bottom side near the leading edge, and a more gradual rise of negative pressure towards the plateau on the top side. A slight increase in the maximum negative pressure on the top side is present. The main difference in geometry between the single and double design point cases is in the higher airfoil camber of the latter.

The full curve gives the pressure distribution for the triple point design. As can be seen, both the upper and lower surface pressure distributions now have a gradual rise towards the plateau. The plateau on the bottom surface is, however, somewhat perturbed due to the conflicting requirements, extending the pressure recovery region over a larger part of the airfoil. The camber of the airfoil is increased with respect to the single design point case, but is lower than for the double design point. The main feature of the triple point design is the larger leading edge radius in comparison to both other cases.

All the three cases were analysed with XFOIL to determine their viscid performance at the Reynolds number $Re = 3 \times 10^6$. The results are shown in Fig. 2. The single design point reaches the minimal drag, but not significantly so. Due to its narrow leading edge, the laminar airflow over the top of the surface is destroyed almost immediately when increasing the angle of attack past its design point (corresponding to the actual viscid lift coefficient $c_l = 0.865$ at this Reynolds number), which manifests itself in the increase of drag and even a slight local drop of the lift coefficient with increasing the angle of attack. Due to the front pressure loading, the airfoil performs well for lift coefficients below its design point.

The double design point case shifts the value of the laminar flow breakdown to higher lift coefficients, and also makes this transition more gradual. More importantly, it allows the airfoil to reach a higher maximum lift coefficient. Favouring higher lift coefficients, does, however, compromise the airfoil performance at the lower lift coefficients. Drag is increased for lift coefficients below about 0.8 when compared to the single design point case.

The triple design point case represents a good compromise. It attains neither the maximum lift to drag ratio ($(c_l/c_d)_{max} = 240$ for the triple, 245 for the double and 233 for the single design point case at the given Reynolds number) nor the minimum drag. Its drag performance at zero lift coefficient, however, is only marginally worse than for the single design point case. Interestingly, its maximum lift coefficient is even higher than for the double design point case. This can be attributed to the larger leading edge radius which is a consequence of the airfoil being optimized over a larger range of lift coefficients.

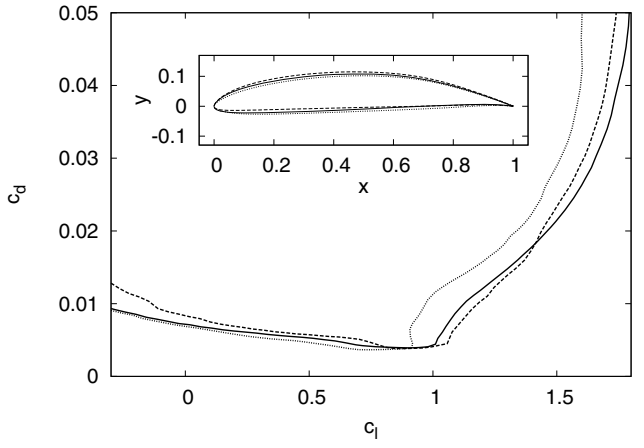

Figure 2: Polar plots at the Reynolds number $Re = 3 \times 10^6$for the series of airfoils as shown in Fig. 1, using the same line types for the various airfoils. The corresponding airfoil geometries are given in the inset.

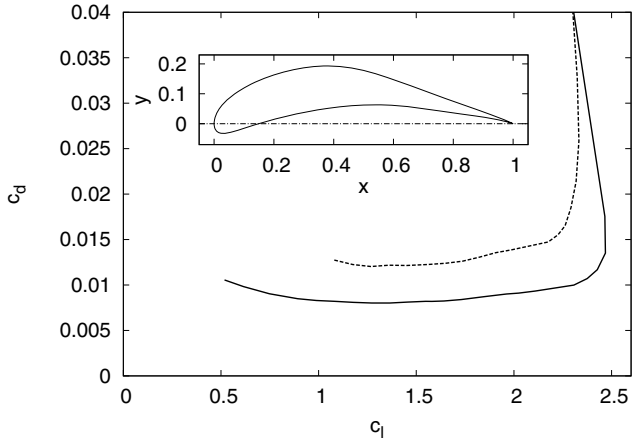

Figure 3: Polar plots for the high lift airfoil of 15% thickness and design lift coefficient $c_l = 2.5$ as shown in the inset for the Reynolds numbes $Re = 3 \times 10^6$ (solid) and $Re = 10^6$ (dashed).

To show the versatility of the method, it was applied in order to design a high lift airfoil with the design lift coefficient $c_l = 2.5$ and a prescribed 15% thickness. A triple point design was used with the offset angles $\Delta\alpha_{1,2} = \pm 1/(2\pi)$ and the weights $\rho_{1,2} = 1/10$ in order to increase the operating range of the airfoil. The pressure recovery parameters were $\mu = 2.5$, $\nu = 3$, $p_0 = 3/5$ and $\delta p = 1/5$. The main difference to the previous case is the choice of the parameter ν, which was chosen such that the pressure recovery shape as given by Eq. 10 follows the asymptotic form as presented by Liebeck and Ormsbee (1970) for large x. The shape of the obtained airfoil and its polar plots as given by XFOIL are shown in Fig. 3. The resulting airfoil shape is highly cambered. The airfoil attains the maximum lift coefficient of about $c_l = 2.47$ at the Reynolds number $Re = 3 \times 10^6$ and $c_l = 2.33$ at $Re = 10^6$. While the boundary layer theory breaks down in the cases of large separations, the maximum lift coefficient as obtained from it can nevertheless still be of interest as a relative comparison number, especially in the regime somewhat below the "peak" value where the boundary layer theory is still adequate. The corresponding maximum lift to drag ratios are $(c_l/c_d)_{max} = 238$ and $(c_l/c_d)_{max} = 152$, respectively.

The pressure distribution for this airfoil is given in Fig. 4. Again flat pressure distributions are favoured, with the multi point design ensuring that the rise to both plateaus near the leading edge is gradual. The pressure recovery on the top surface is governed by the corresponding constraint. On the bottom surface, the pressure distribution tends to remain constant and then gradually rises closer to the freestream value near the trailing edge. Such a distribution is qualitatively similar to those employed by Liebeck and Ormsbee (1970).

It is of interest whether the outlined procedure is capable of resulting in airfoils similar to those that are already successfully used in practice. As an example, an airfoil as used on the Pipistrel series of aircraft, such as the Virus model that recently won the most categories in the NASA Centennial Challenge competition[2], is taken. The set of parameters for the cost function (Eq. 3) that, when minimized, results in an airfoil that matches the real one as closely as possible is given by the the design lift coefficient of 0.45, the thickness of 17% and using an additional design point that is offset by an angle of attack $\Delta\alpha_1 = 1/(2\pi)$ with the weight $\rho_1 = 1/3$. The pressure recovery constraint parameters were $\mu = 1.5$, $\nu = 1$, $p_0 = 0.6$ and $\delta p = 0.05$.

The comparison of the calculated and the actual airfoil is given in Fig. 5. Not only are the general features of the two airfoils similar, but the actual contours match closely as well. The airfoil resulting from the optimization procedure clearly

[2] 2007 NASA Personal Air Vehicle Challenge, `http://cafefoundation.org/`

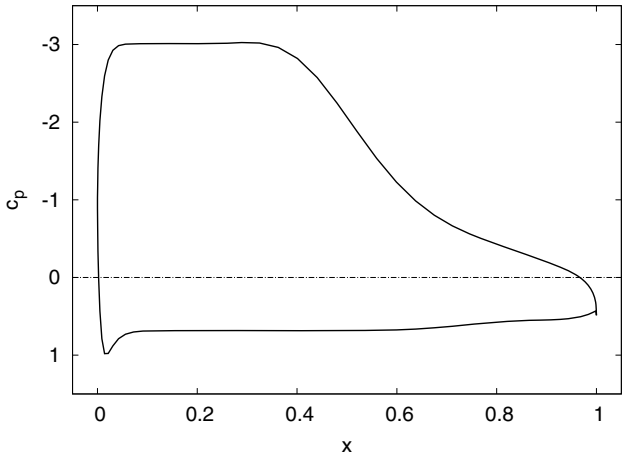

Figure 4: The pressure distribution ($c_p = 1 - v^2$) for the airfoil as shown in Fig. 3 at its design point $c_l = 2.5$.

reproduces the basic features such as slight aft pressure loading of the actual airfoil and the different rise towards the plateaus of the pressure distribution on the top versus the bottom side. The largest difference between the two airfoils can be seen in the aft section of the bottom side, where the calculated airfoil remains wider and therefore allows for a faster pressure recovery than can be found on the actual airfoil. It should be stressed that the optimization procedure only takes a very small number of parameters in order to obtain the airfoil shape. Apart from tweaking these few parameters in order to obtain as close a match as possible, there was no input from the real airfoil data into the optimization procedure, not even as a starting point for the calculation.

5 Conclusion

The procedure as outlined in this paper allows for automatic calculation of low speed airfoils that conform to some of the typical design principles. As the automatic optimization is performed by using a parameter free cost function and a number of constraints with few parameters, the procedure requires little input from the designer. The procedure can also be easily generalized to multiple design points, resulting in airfoils that perform well over a range of angles of attack. While classical design methods already provide the means to design excellent airfoils, the proposed method is most useful in situations where there is a need to design a large

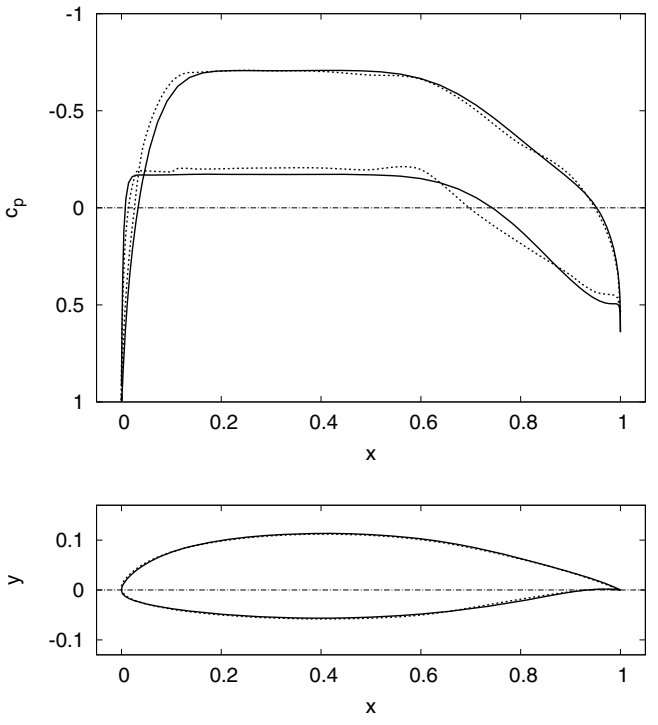

Figure 5: The comparison of the airfoil as used on the Pipistrel series of aircraft (dotted) with the computed shape (full) is shown in the bottom picture. The pressure distribution for the computed airfoil (full) and the existing airfoil (dotted) at the design lift coefficient $c_l = 0.45$ is given in the top picture.

number of similar airfoils with continuously varying design points, such as those along different cross sections of a wing or a propeller.

The cost function as chosen here was deliberately as simple as possible while still producing desirable results. A single, low parameter cost function is unlikely to satisfy all the possible airfoil design requirements. It is easy to extend the outlined method towards additional demands. One possible modification is to introduce a bias to the pressure gradient in the cost function (Eq. 1) such that favourable (rather than zero) pressure gradients are optimal. On the other hand, for transonic design it might be better to simply use the maximum negative pressure reached at the surface of airfoil as the cost function.

The cost function in Eq. 1 can also be expressed as an integral over a surface in

three dimensions. It remains a problem for the future whether such a cost function might extend the procedure from the design of airfoils to the design of full three-dimensional bodies.

References

Amirante, R.; Catalano, L. A.; Dadone, A.; Daloiso, V. S. E. (2007): Design Optimization of the Intake of a Small-Scale Turbojet Engine. *CMES: Computer Modeling in Engineering and Sciences*, vol. 18, no. 1, pp. 17–30.

Anderson Jr., J. D. (2007): *Fundamentals of Aerodynamics*. McGraw-Hill, Singapore.

Bartels, R. H.; Beatty, J. C.; Barsky, B. A. (1998): *An Introduction to Splines for Use in Computer Graphics and Geometric Modelling*, chapter 10. Morgan Kaufmann, San Francisco, 1998.

Drela, M.; Giles, M. B. (1987): Viscous-inviscid analysis of transonic and low Reynolds number airfoils . *AIAA Journal*, vol. 25, pp. 1347–1355.

Eppler, R. (1991): *Airfoil Design And Data*. Springer-Verlag, Berlin.

Fedelinski, P.; Gorski, R. (2006): Analysis and optimization of dynamically loaded reinforced plates by the coupled boundary and finite element method. *CMES: Computer Modeling in Engineering and Sciences*, vol. 15, no. 1, pp. 31–40.

Jiang, C.; Han, X. (2007): A New Uncertain OptimizationMethod Based on Intervals and An ApproximationManagementModel. *CMES: Computer Modeling in Engineering and Sciences*, vol. 22, no. 2, pp. 97–118.

Jimenez-Octavio, J.; Lopez-Garcia, O.; Pilo, E.; Carnicero, A. (2008): Coupled Electromechanical Optimization of Power Transmission Lines. *CMES: Computer Modeling in Engineering and Sciences*, vol. 25, no. 2, pp. 81–97.

Lamberti, L.; Pappalettere, C. (2007): Weight Optimization of Skeletal Structures with Multi-Point Simulated Annealing. *CMES: Computer Modeling in Engineering and Sciences*, vol. 18, no. 3, pp. 183–221.

Lewis, R. I. (1991): *Vortex Element Methods for Fluid Dynamic Analysis of Engineering Systems*. Cambridge University Press, Cambridge.

Liebeck, R. H.; Ormsbee, A. I. (1970): Optimization of Airfoils for Maximum Lift. *Journal of Aircraft*, vol. 7, pp. 409–416.

Lighthill, M. J. (1945): A New Method of Two-Dimensional Airfoil Design. Technical Report 2112, Aeronautical Research Council, R&M, 1945.

Mantia, M. L.; Dabnichki, P. (2008): Unsteady 3D Boundary Element Method for OscillatingWing. *CMES: Computer Modeling in Engineering and Sciences*, vol. 33, no. 2, pp. 131–153.

Medic, G.; Mohammadi, B.; Petruzzelli, N.; Stanciu, M.; Hecht, F. (1999): 3D Optimal Shape Design for Complex Flows: Application to turbomachinery. *AIAA Paper*, vol. 99-0833.

Nocedal, J.; Wright, S. J. (2007): *Numerical Optimization*. Springer-Verlag, New York.

Papalambros, P. Y.; Wilde, D. J. (2000): *Principles of Optimal Design: Modeling and Computation*. Cambridge University Press, Cambridge.

Press, W. H. (2007): *Numerical Recipes: The Art of Scientific Computing*. Cambridge University Press, Cambridge.

Selig, M. S.; Maughmer, M. D. (1992): Multipoint inverse airfoil design method based on conformal mapping. *AIAA Journal*, vol. 30, pp. 1162–1170.

Sellountos, E.; Sequeira, A. (2008): A HybridMulti-Region BEM / LBIE-RBF Velocity-Vorticity Scheme for the Two-Dimensional Navier-Stokes Equations. *CMES: Computer Modeling in Engineering and Sciences*, vol. 23, no. 2, pp. 127–147.

Strand, T. (1973): Exact Method of Designing Airfoils With Given Velocity Distribution in Incompressible Flow. *Journal of Aircraft*, vol. 10, pp. 651–659.

Appendix A: Implementation of the panel method

The ideal incompressible flow around an airfoil is calculated by the constant vorticity panel method [Lewis (1991)]. Such boundary element methods still attract significant attention in fluid dynamics today [Sellountos and Sequeira (2008),Mantia and Dabnichki (2008)]. Each panel i has an assigned vorticity density γ_i. The value of γ_i is also equal to the tangential velocity of the flow at the boundary. The velocity contribution of each panel with the center $\mathbf{c}_i$, length a_i, unit tangent vector $\mathbf{t}_i$ and unit normal vector $\mathbf{n}_i$ to the total flow is calculated as

$$\mathbf{v}_i = v_t \mathbf{t}_i + v_n \mathbf{n}_i, \tag{13}$$

$$v_t = \frac{1}{2\pi}\left(\tan^{-1}(x_n, x_t - a_i/2) - \tan^{-1}(x_n, x_t + a_i/2)\right), \tag{14}$$

$$v_n = \frac{1}{4\pi}\left(\ln\left[\frac{(x_t - a_i/2)^2 + x_n^2}{(x_t + a_i/2)^2 + x_n^2}\right]\right) \tag{15}$$

with

$$x_t = (\mathbf{r} - \mathbf{c}_i)\cdot\mathbf{t}_i,\ x_n = (\mathbf{r} - \mathbf{c}_i)\cdot\mathbf{n}_i. \tag{16}$$

The function $\tan^{-1}(y,x)$ with the range $[-\pi,\pi)$ is the polar angle function for the coordinates x and y and is equal to $\tan^{-1}(y/x)$ in the first and the fourth quadrant.

The boundary condition requires that the tangential velocity on the internal side of the boundary should equal 0. If the velocity far away from the airfoil equals $\mathbf{v}_0$, this leads to the system of N equations for N panel vorticities

$$\sum_{j=1}^{N} A_{ij}\gamma_j = \mathbf{v}_0\cdot\mathbf{t}_i \tag{17}$$

where

$$A_{ij} = -\mathbf{t}_i\cdot\mathbf{v}_j, i \neq j,\ \ A_{ii} = \frac{1}{2}. \tag{18}$$

If the panels closest to the trailing edge are given the indices 1 and N, then the Kutta condition is expressed as

$$\gamma_1 + \gamma_N = 0, \tag{19}$$

This, however, leads to an overdetermined system $N+1$ equations for N unknowns. The solution employed here is to perform a quasi inversion of the now non-square matrix A_{ij} using the singular value decomposition (see e.g. Press (2007)). While in principle a quasi inverse would lead to a solution only approximately satisfying all the equations, it is important to note that the square system of equations without the Kutta condition is actually underdetermined, since the ideal flow solution can admit an arbitrary total vorticity. This means that the quasi inverse will actually be able to satisfy all of the conditions since the Kutta condition merely fixes the existing vorticity degree of freedom in the square system of equations.

Once the system is solved, the lift coefficient is given by the total vorticity as

$$c_l = 2\sum_{j=1}^{N}\gamma_i a_i. \tag{20}$$

Appendix B: Minimization implementation

In order to perform the minimization of a function $\tilde{f}(\mathbf{z})$ over the variables $\mathbf{z}$ under the constraints $c_l(\mathbf{z}) = g_1(\mathbf{z}) = g_{1,0}$, $t_{\max}(\mathbf{z}) = g_2(\mathbf{z}) = g_{2,0}$ and $r(\mathbf{z}) = g_3(\mathbf{z}) = g_{3,0} = 0$, where $g_{j,0}$ are specified constants, the calculation of gradients with respect to $\mathbf{z}$ must be performed for the cost function as well as all the constraints. These gradients are denoted as $\nabla\tilde{f}$, ∇g_1, ∇g_2 and ∇g_3 and are calculated numerically by offsetting each variable x_i of the vector $\mathbf{z}$ by a small ε and performing a finite difference approximation for the derivative. Choosing too small an ε will cause numerical instabilities. The value $\varepsilon = 10^{-4}$ was used throughout.

In order to keep the search constrained, the descent should not follow $\nabla\tilde{f}$ but only its component that is orthogonal to all constraint gradients ∇c_j. On each calculation of a new gradient, its projection $\overline{\nabla\tilde{f}}$ is calculated such that $\overline{\nabla\tilde{f}} \cdot \nabla g_j = 0$ for all $j = 1, \ldots, m$, where m is the number of constraints (3 in the present example). This is performed by solving the system of m equations for each i,

$$\sum_{j=1}^{m} (\nabla g_i) \cdot (\nabla g_j) \lambda_j = (\nabla\tilde{f}) \cdot (\nabla g_i), \tag{21}$$

in order to obtain the constrained gradient

$$\overline{\nabla\tilde{f}} = \nabla\tilde{f} - \sum_{j=1}^{m} \lambda_j \nabla g_j. \tag{22}$$

The system (Eq. 21) can be solved directly, or iteratively by a repeated projection of the current solution vector along the directions of each constraint gradient ∇c_l, where the starting solution vector is the unconstrained cost function gradient. This amount exactly to the Gauss-Seidel iteration for the system (Eq. 21).

A linear minimum search is then performed in the direction of $\overline{\nabla\tilde{f}}$. Since the constraints g_j will in general not be linear functions of search coordinates, drifts from the specified constraint values will occur spontaneously while following the search direction $\overline{\nabla\tilde{f}}$, which is calculated at a single point on the line. Since, during each linear search, the constraint gradients are nevertheless not expected to deviate significantly from the initial values, after each step to obtain the n-th iteration for the variables $\mathbf{z}$, a number of repeated additional correction steps is performed

$$\overline{\mathbf{z}}_n = \mathbf{z}_n - \sum_{j=1}^{m} \Delta g_j \frac{\nabla g_j}{|\nabla g_j|^2}, \tag{23}$$

where

$$\Delta g_j(\mathbf{z}) = g_j(\mathbf{z}) - g_{j,0} \tag{24}$$

is the error in the constraint function. This will not lead to the constraints being satisfied exactly during each step of the search, but once convergence is approached the correction steps become more efficient and lead to a converging final solution.

The inexact linear search along a chosen direction was performed by taking steps of finite size along the projected gradient direction, starting from a small step size ($|\delta \mathbf{z}| = 10^{-4}$ was chosen), applying the above correction step each time and then increasing the step size by a fixed multiplication factor ($\beta = 3/2$ in the present example) until the step size $|\delta \mathbf{z}|$ became larger than some number ($|\delta \mathbf{z}| < 10^{-2}$ in present calculations), and from there on the step size was kept constant. Upon reaching a local minimum for the cost function on this set of points, a new search is started by repeating the gradient calculations from the obtained minimal point. Typicially a few ten recalculations of the gradient direction are sufficient for finding a reasonable solution, while about a few hundred are needed for convergence within the prescribed variable step $|\delta \mathbf{z}|$.